



UNIVERSITY OF LEEDS

This is a repository copy of *Probing the Spiral Magnetic Phase in 6 nm Textured Erbium using Polarised Neutron Reflectometry*.

White Rose Research Online URL for this paper:

<https://eprints.whiterose.ac.uk/107305/>

Version: Accepted Version

---

**Article:**

Satchell, N [orcid.org/0000-0003-1597-2489](https://orcid.org/0000-0003-1597-2489), Witt, JDS [orcid.org/0000-0001-5018-415X](https://orcid.org/0000-0001-5018-415X), Burnell, G [orcid.org/0000-0002-9486-0639](https://orcid.org/0000-0002-9486-0639) et al. (5 more authors) (2016) Probing the Spiral Magnetic Phase in 6 nm Textured Erbium using Polarised Neutron Reflectometry. *Journal of Physics: Condensed Matter*, 29 (5). 055801. pp. 1-5. ISSN 0953-8984

<https://doi.org/10.1088/1361-648X/29/5/055801>

---

© 2016 IOP Publishing Ltd. This is an author-created, un-copied version of an article accepted for publication/published in *Journal of Physics: Condensed Matter*. IOP Publishing Ltd is not responsible for any errors or omissions in this version of the manuscript or any version derived from it. The Version of Record is available online at <https://doi.org/10.1088/1361-648X/29/5/055801>.

**Reuse**

Items deposited in White Rose Research Online are protected by copyright, with all rights reserved unless indicated otherwise. They may be downloaded and/or printed for private study, or other acts as permitted by national copyright laws. The publisher or other rights holders may allow further reproduction and re-use of the full text version. This is indicated by the licence information on the White Rose Research Online record for the item.

**Takedown**

If you consider content in White Rose Research Online to be in breach of UK law, please notify us by emailing [eprints@whiterose.ac.uk](mailto:eprints@whiterose.ac.uk) including the URL of the record and the reason for the withdrawal request.



[eprints@whiterose.ac.uk](mailto:eprints@whiterose.ac.uk)  
<https://eprints.whiterose.ac.uk/>

# Probing the Spiral Magnetic Phase in 6 nm Textured Erbium using Polarised Neutron Reflectometry

N. Satchell,<sup>1,2,\*</sup> J. D. S. Witt,<sup>1</sup> G. Burnell,<sup>1,†</sup> P. J. Curran,<sup>3</sup>  
C. J. Kinane,<sup>2</sup> T. R. Charlton,<sup>2,‡</sup> S. Langridge,<sup>2</sup> and J. F. K. Cooper<sup>2</sup>

<sup>1</sup>*School of Physics and Astronomy,  
University of Leeds, Leeds, LS2 9JT, United Kingdom*

<sup>2</sup>*ISIS, STFC Rutherford Appleton Laboratory,  
Chilton, Didcot, Oxon, OX11 0QX, United Kingdom*

<sup>3</sup>*Department of Physics, University of Bath,  
Claverton Down, Bath, BA2 7AY, United Kingdom*

(Dated: October 20, 2016)

## Abstract

We characterise the magnetic state of highly-textured, sputter deposited erbium for a film of thickness 6 nm. Using polarised neutron reflectometry it is found the film has a high degree of magnetic disorder, and we present some evidence that the films' local magnetic state is consistent with bulk-like spiral magnetism. This, combined with complementary characterisation techniques, show that thin film erbium is a strong candidate material for incorporation into device structures.

## INTRODUCTION

The most important magnetic interaction in Er (like other heavy rare earth (RE) metals), is the isotropic Ruderman-Kittel-Kasuya-Yosida (RKKY) exchange interaction. This results in a minimised free energy when the ferromagnetism consists of sheets perpendicular to the  $c$ -axis, with the moments rotating through a certain angle from one sheet to the next. Competing with this are a magnetoelastic contribution and the crystalline anisotropy in the hcp structure, which favour magnetic interaction either along or perpendicular to the  $c$ -axis. In Er, the crystalline anisotropy results in a complex temperature dependence, with an initial ordering of moments parallel to the  $c$ -axis, followed at lower temperatures by a canting out-of the  $c$ -plane; this creates a rich magnetic phase diagram [1–9].

Bulk Er has three distinct magnetic transitions. Within the three magnetic phases there are many other reproducible (but metastable) commensurate states. On cooling below the high-temperature paramagnetic phase ( $\approx 85$  K) Er first gains a sinusoidal,  $c$ -axis modulated (CAM) antiferromagnetic phase with a wavelength of about 7 atomic layers (which is labelled by the magnetic wave vector  $\tau_c = 2/7$ , in units of reciprocal lattice parameter,  $c^*$ ). As the temperature is lowered the magnetic wave vector of the CAM peaks at  $\approx 52$  K. Below this temperature Er enters an ‘intermediate’ canted helical phase where the in-plane moments begin to order creating what has been referred to by Cowley *et al.* as an antiferromagnetic “wobbling cycloid” [1]. The magnetic repeat distance increases with decreasing temperature, through a number of stable commensurate phases, to 8 atomic layers ( $\tau_c = 1/4$ ). These states exhibit a ferrimagnetic moment. Finally, below 18 K a conical  $c$ -axis ferromagnetic phase is formed with a wavevector ( $\tau_c = 5/21$ ). We have been able to confirm that many of the magnetic states of bulk Er are reproducible in sputter deposited epitaxial thin films of thickness 200 nm [9].

In order to become device relevant in the field of spintronics, as a spin transfer torque (STT) material (as theoretically postulated by [10]) it is of key importance that Er retains its spiral magnetisation upon reduction of thickness below 10 nm. For the emerging field of superconducting spintronics, Er is a strong candidate material to be the necessary source of inhomogeneous ferromagnetism [11, 12]. In our previous work on 50 and 200 nm thick Er films, neutron diffraction was used to study magnetic Bragg peaks generated by the repeating magnetic structure. These gave direct information about the magnetic state of

the films. On reduction of the Er thickness to 6 nm, the magnetic Bragg peak was too weak to be detected. For this thinner sample, we used polarised neutron reflectometry to extract depth dependent magnetisation profiles presented in this work.

## METHODS

The Er film was deposited using DC sputtering in a system with substrate heaters. At the highest temperature, the base pressure of the system was  $\approx 10^{-7}$  mbar. This pressure improves as the system temperature is lowered. The sample was grown on 0.65 mm thick *c*-plane Al<sub>2</sub>O<sub>3</sub> substrate. 10 nm of Nb was deposited at a nominal temperature of 700°C, after which the system was cooled to 500°C and 6 nm of Er and then a 5 nm-thick Lu capping layer were deposited. Growth was performed in an Ar atmosphere with a typical Ar flow of 55 sccm and pressure of 2-3 mbar, at a substrate-sample distance of 70 mm, and at a typical growth rate of 0.1 nm s<sup>-1</sup>. Growth rates were calibrated by fitting to Keissig fringes obtained by X-ray reflectometry to Nb films, and bilayers of Nb/Lu and trilayers of Nb/Er/Lu. The Nb was grown first as it has been shown to be an effective buffer layer for the growth of rare-earth metals [13]. The Nb/Er interface is known to be sharp due to the lack of alloying and intermixing between Nb and Er [14]. It was found that traditional capping metals (Ta, Nb, etc) tended to form islands on the surface of the Er layer, and did not protect the layer from oxidation. Lu has good lattice matching with Er, and was found to grow as a continuous layer on top of Er. It was therefore a much more effective capping material and protects the Er from oxidation.

Magnetisation loops were measured using an 6 T SQUID magnetometer. Polarised neutron reflectometry (PNR) was performed on the PolRef beamline at the ISIS neutron and muon source. X-ray diffraction (XRD) and reflectometry (XRR) were performed on a Rigaku SmartLab diffractometer at the ISIS R53 characterisation lab. X-ray and polarised neutron reflectometry data were analysed using the GenX software [15].

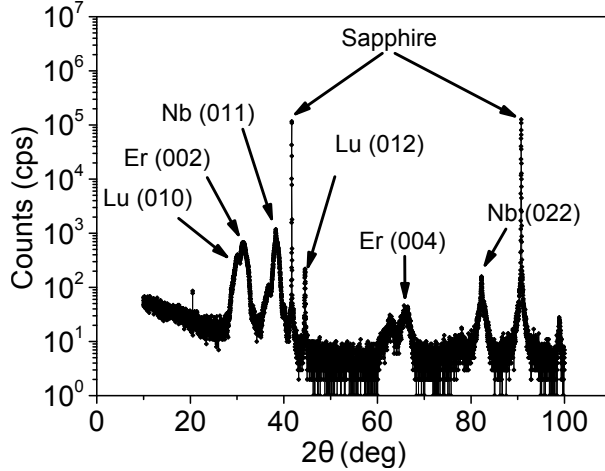


FIG. 1. X-ray diffraction of the textured Er thin film, with the main structural peaks indicated.

## RESULTS

### X-ray Diffraction

Structural characterisation was performed using XRD, and can be seen in Figure 1. The sample shows strong structural Bragg peaks, identified in the figure, and there is no evidence for  $\text{Er}_2\text{O}_3$  formation. The grain size perpendicular to the plane of the film is then estimated using the Scherrer equation [16] for each layer. As neutron reflectivity is not sensitive to in-plane structural coherence, only grains perpendicular to normal are considered. The Nb (100) buffer layer has grain size of 8 nm and the Er (002) phase has 6 nm grain size, indicating very high structural coherence for both layers. The Lu layer shows some degree of texture, however is likely to also form a layer of LuO on the film surface. As its role is only to protect the Er from oxidation the morphology of this film is not of importance and hence not optimised in this study.

For the Er films in heteroepitaxial growth, lattice mismatching between Nb and Er will translate a Bragg peak from the ideal angle. Non-uniform strain can cause the peak to broaden and may be mistaken for a reduction in grain size. As the out-of-plane grain size approximately matches the film thickness, it is assumed this is not the case, and that any strain in the Er layer is uniform. The Er grows epitaxially on the most densely packed Nb (110) plane, in the Nishiyama-Wasserman orientation. The in-plane axis of hcp Er  $[10\bar{1}0]$  is aligned with bcc Nb  $[\bar{1}10]$  with 3:4 supercell commensuration in their nearest-neighbour

Layer	Density (f.u./Å <sup>3</sup> )	Thickness (Å)	$\sigma$ (Å)
LuO	0.030	12	6
Lu	0.033	35	2
Er	0.030	67	5
Nb	0.055	84	3
Al <sub>2</sub> O <sub>3</sub>	0.065	$\infty$	3

TABLE I. Material parameters extracted from the fit in fig. 2. The error in the extracted values is approximately 10%.

distances along these axes [13]. While direct measurement of the in-plane lattice parameters were not available for this work, using our previous work as a guide [9], in-plane strain on the Er [10 $\bar{1}$ 0] from the Nb [ $\bar{1}$ 10] (which is in turn strained by the Al<sub>2</sub>O<sub>3</sub> substrate) could be as large as -1.8 %. In the  $c$ -axis, the measured lattice spacing of  $5.71 \pm 0.02$  Å is quite different than the expected 5.585 Å, indicating a strain of +2.24 %. This  $c$ -axis extension is consistent with an in-plane contraction and can be reduced, towards the bulk value, by increasing Er film thickness [9]. The addition of a Y buffer layer between the Nb and Er can cause the opposite effect, a contraction in the measured  $c$ -axis lattice parameter [17].

### X-ray Reflectometry

The nominal *as-grown* structure was Al<sub>2</sub>O<sub>3</sub> (substrate) / Nb (10 nm) / Er (6 nm) / Lu (5 nm). The XRR data and model fit from this representative sample can be seen in Figure 2. The approach to modelling the XRR was to keep the model no more complicated than needed and to concentrate on correctly fitting data in the Q range accessible by PNR. The addition of many further layers to the model (in an effort to improve the fit to the data) risks producing an unphysical representation of the sample.

The extracted parameters are shown in Table I. There is good agreement between the modelled values and the nominal structure when only one additional layer is introduced to account for expected post growth oxidation of the capping layer. The interfacial roughness is small for all layers. Of particular note for this work is the low interfacial roughness ( $\sigma$ ) between the Nb layer and the adjacent Er layer, indicating a lack of intermixing.

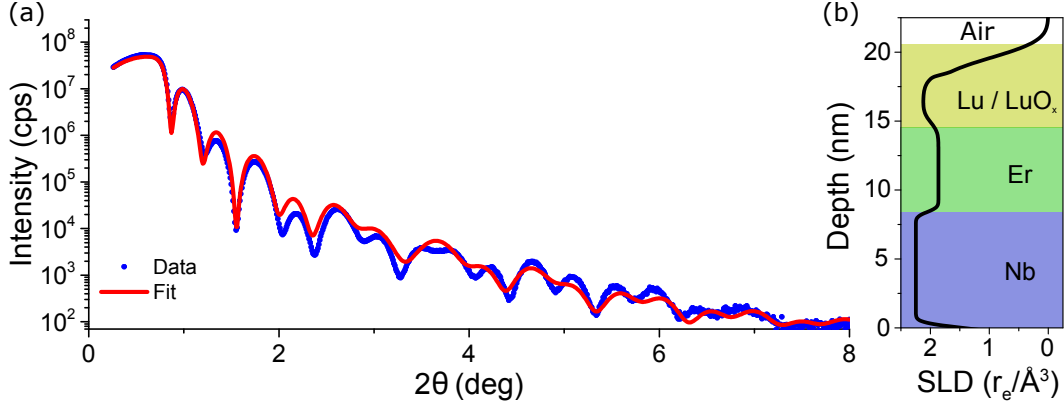


FIG. 2. (a) Low-angle X-ray reflectometry and corresponding fit. (b) The SLD (in units of classical electron radius ( $r_e$ ) per  $\text{\AA}^3$ ) with depth from the fit in (a). The returned fit parameters are given in Table I.

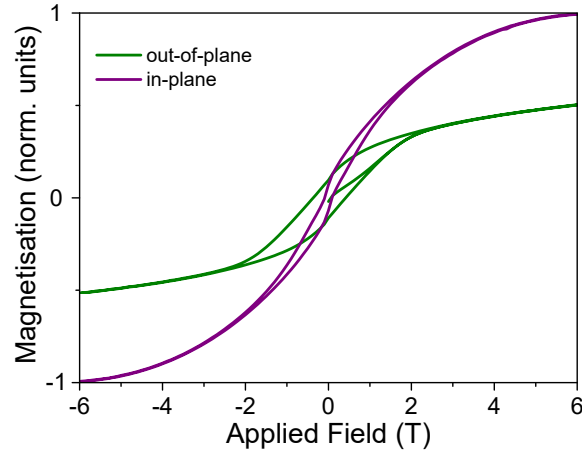


FIG. 3. Magnetic hysteresis loops measured in and out-of the sample plane. Loops were acquired at a temperature of 5 K.

### Magnetic Characterisation

In thin film Er of this thickness range, previous characterisation work has shown that the conical magnetic state of bulk crystals is largely suppressed, placing the film in the intermediate canted helical state [9].

Both in and out-of-plane magnetisation hysteresis loops for the Er film at 5 K can be seen in Figure 3. Although normalised in the figure for clarity, the magnetisations at 6 T,  $M_{6T}$ , differ in each configuration. The in-plane  $M_{6T} = 2900 \pm 200 \text{ emu/cm}^3$  is comparable

to the theoretical maximum  $M_s = 2700 \text{ emu/cm}^3$  (within errors). This is much larger than the out-of-plane  $M_{6T} = 1500 \pm 100 \text{ emu/cm}^3$ .

This is strong evidence that, for this thickness range, the long-ranged ordering is perturbed at the interfaces, making the film more susceptible to in-plane fields capable of unwinding the helical state, causing saturation completely along this direction. This is likely due to the dominance of surfaces disrupting the long ranged RKKY interaction. The weakening of RKKY at the surface makes surface moments easier to rotate [18, 19]. This in turn causes the nearest neighbours to align with the field also, until the spiral has completely unwound and the sample is saturated.

The field needed to saturate the film out-of-plane is beyond 6 T (the largest available field). This difficulty in saturating the film out-of-plane is dominated by the difficulty in reversing the canting angle and has been shown in previous work to be up to 14 T [1].

It is interesting to note that in both loops the squareness ratio is low, with only a small fraction of  $M_{6T}$  retained at remanence. The expected canted helical state would result in a small net out-of-plane component at remanence. In-plane remanence results from incomplete helices. Upon relaxing the field this suggests that the sample returns to its initial (as grown) phase or a nearly compensated non-collinear state. The in-plane loop shows a wasp-waisted feature, which can imply some coupling between magnetic phases with different coercivity. This is consistent with the anisotropy of the surface moments being weaker than the bulk.

The key aspect for the interpretation of the PNR is twofold. Firstly, that the Er retains a bulk like moment above  $9 \mu_B/\text{atom}$  and secondly, that this large moment is mostly compensated to give a low net average remanent moment.

This behaviour is quite different to its neighbour in the periodic table holmium, which in thin films saturates in-plane at fields of typically only 300 mT, after which the squareness of its hysteresis loop suggest a long-ranged ferromagnetic ordering takes over and spiral magnetism does not reform [18, 20]. This difference is most likely due to the  $c$ -axis crystalline anisotropy in the hcp structure being more important, or certainly being retained to a greater extent, in thin film Er.

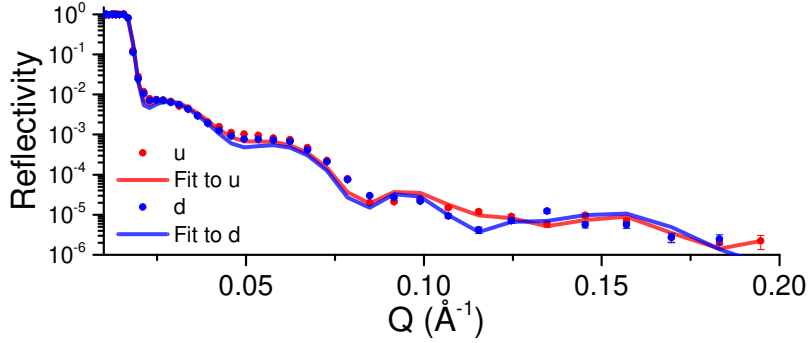


FIG. 4. Polarised neutron reflectometry curves from the 6nm Er film. The two neutron spin states are shown (u,d) along with the corresponding fit described in the text. Curves were acquired at a temperature of 5 K in a 10 mT field.

### Polarised Neutron Reflectometry

By measuring the neutron reflectivity as a function of the wavevector transfer and neutron spin eigenstate, PNR allows the scattering length density (SLD) to be obtained. Careful fitting to the two obtained reflectivity curves in PNR allows the extraction of depth dependent magnetisation. Structural information can also be extracted, but in this work the XRR model was imported as a starting point for the fit. PNR has been widely employed in the successful characterisation of spintronic materials [21].

Figure 4 shows the obtained PNR curves for the sample with the corresponding fit to each spin state. The structural properties were imported from the XRR fit and the magnetisation of each layer was a fitting parameter. Despite the in-plane saturation moment of the sample being high (consistent with bulk), there appears to be very little splitting between the two spin states in the PNR data. This is also seen in the spin asymmetry (Figure 5 (a)) which is the difference between the two spin states normalised to their sum.

The sample was field cooled to a temperature 5 K in a 10 mT in-plane field needed to guide the neutrons. At this field and temperature, Er is expected to be in a highly non-collinear or spiral magnetic phase. It is not expected field cooling in such a small applied field will have an impact on the magnetic state of the Er. As fields much larger than the maximum available field on the beamline would be needed to change the magnetic state of the Er, the 10 mT applied field was maintained for the measurement. Atomic scale anti-ferromagnetism is too short a lengthscale for neutron reflectivity to probe, and as such is seen as net zero

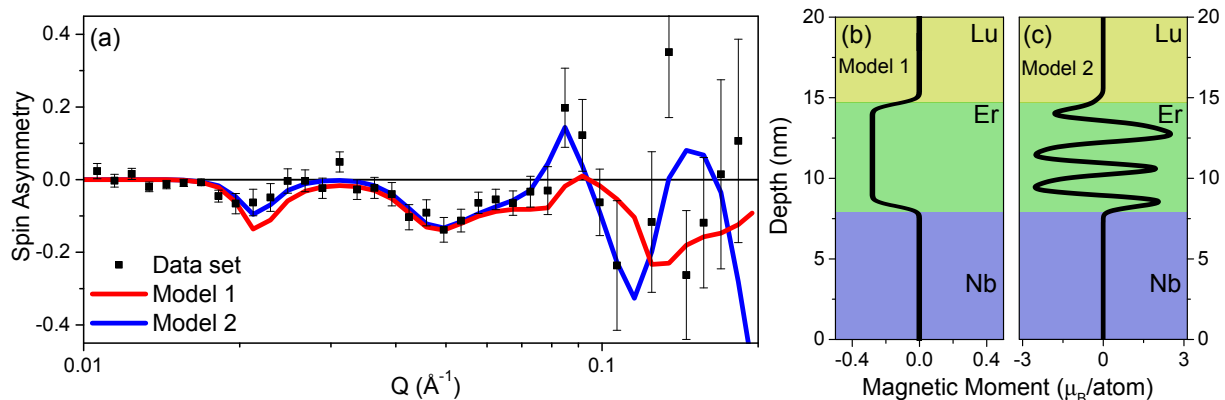


FIG. 5. (a) Spin asymmetry for the PNR data in Figure 4 with two models (see text) for the magnetism in the Er layer. The magnetic depth profile for model 1 is plotted in (b) and model 2 in (c).

moment. In Er, however, the spiral repeat distance (equivalent to the anti-ferromagnetic lengthscale) is several atomic layers long; this is still too short for full depth dependence, but allows some insight. The Er (as with most RE ferromagnets) is likely to contain chiral magnetic domains [22, 23]. The measurement technique employed in this work, however, will not be sensitive to the chirality of the domains.

Two fitting techniques are employed on the data. The first technique treats the magnetic moment inside the Er layer as being constant with depth, and will return the average moment inside the Er (model 1). The second technique allows the moment to be a depth dependent free parameter (model 2). In both cases, positive magnetisation corresponds to moments pointing in the direction of applied field. For a saturated, ordered, ferromagnet both fitting techniques would return that the magnetisation of the entire layer is positive.

The spin asymmetry and results of the two fitting techniques are presented in Figure 5. The differences between the two models are too subtle to observe in the reflectivity data, and even in the spin asymmetry there are only very small differences at low  $Q$ . Notably at higher  $Q$  ( $> 0.08\text{\AA}^{-1}$ ) the models begin to separate, with model 2 providing a closer fit in this region.

Model 1 (shown in Figure 5 (b)) returns a constant magnetic moment inside the sample of  $-0.3 \mu_B/\text{atom}$ . This is far lower than the moment possessed by the individual Er atoms (over  $9 \mu_B/\text{atom}$ ). The returned moment is also negative. This solution is therefore likely

a returned ‘average’ magnetisation due to an inhomogeneous magnetic state within the Er layer.

Model 2 (shown in Figure 5 (c)) returns a small total moment, but a large, oscillating, depth dependent internal moment. The oscillation between positive and negative magnetisation values returned from this fitting technique is a good approximation for spiral magnetisation inside the Er layer. The average moment of this model (returned by integration) is  $-0.26 \pm 0.05 \mu_B/\text{atom}$ , consistent with the returned moment for model 1.

This model appears to have given some additional insight into the local magnetic state. It returns a magnetic spiral with repeat distance of  $\approx 2.5$  nm. This corresponds to a magnetic repeat distance of 4.3 atomic layers. Examining the expected bulk phases of Er, this is not consistent with any known commensurate state.

In order to interpret which of the two models provides the most insight into the actual magnetic state of the sample, one needs to consider the magnetometry. This showed the thin Er layer retained a high moment per atom in addition to a low net average remanent moment. Both models predict the latter, but only the spiral model predicts the former and is hence a candidate for the non-collinear state of the system. Even if the returned model does not match the exact magnetic state of the sample, the PNR shows evidence that the magnetisation of this sample is highly disordered.

## CONCLUSIONS

In summary, we have found from the PNR technique that the internal magnetic state of the 6 nm thick Er film is highly inhomogeneous. From magnetic measurements the application of a 6 T field in-plane can ‘unwind’ the inhomogeneity and the film reaches its bulk magnetisation. Relaxing the field causes the film to return to the inhomogeneous state, with only very small remanent magnetisation. Fitting the PNR data shows that the Er is in a highly non-collinear magnetic state, with an average moment of just  $-0.3 \mu_B/\text{atom}$  compared to a bulk moment  $> 9 \mu_B/\text{atom}$ . This is consistent with the Er film retaining a magnetic spiral state, though this state cannot be conclusively proven. The fact that the magnetic state is highly disordered shows Er as a promising candidate material for incorporation into spintronic, and superconducting spintronic, device structures in the future.

The authors would like to thank the UK EPSRC (grant numbers: EP/J010634/1 and

EP/J010650/1) for their financial support. The ISIS neutron and muon source for allocating beamtime (RB:1410611). NS acknowledges JEOL Europe and ISIS for PhD funding.

The data associated with this paper are openly available from the University of Leeds data repository. <http://doi.org/10.5518/93>

---

\* nathan.satchell@stfc.ac.uk

† g.burnell@leeds.ac.uk

‡ Present address: Quantum Condensed Matter Division, Oak Ridge National Lab, Oak Ridge, TN 37831-6473

- [1] R. A. Cowley and J. Jensen, *J. Phys.: Condens. Matter* **4**, 9673 (1992).
- [2] M. Habenschuss, C. Stassis, S. K. Sinha, H. W. Deckman, and F. H. Spedding, *Phys. Rev. B* **10**, 1020 (1974).
- [3] D. Gibbs, J. Bohr, J. D. Axe, D. E. Moncton, and K. L. D'Amico, *Phys. Rev. B* **34**, 8182 (1986).
- [4] H. Lin, M. F. Collins, T. M. Holden, and W. Wei, *Phys. Rev. B* **45**, 12873 (1992).
- [5] D. A. Jehan, D. F. McMorrow, J. A. Simpson, R. A. Cowley, P. P. Swaddling, and K. N. Clausen, *Phys. Rev. B* **50**, 3085 (1994).
- [6] B. Watson and N. Ali, *J. Phys.: Condens. Matter* **7**, 4713 (1995).
- [7] B. Watson and N. Ali, *J. Phys.: Condens. Matter* **8**, 1797 (1996).
- [8] B. H. Frazer, J. R. Gebhardt, and N. Ali, *Journal of Applied Physics* **85**, 6100 (1999).
- [9] J. D. S. Witt, J. F. K. Cooper, N. Satchell, C. J. Kinane, P. J. Curran, S. J. Bending, S. Langridge, L. J. Heyderman, and G. Burnell, Submitted to *Scientific Reports* (2016).
- [10] O. Wessely, B. Skubic, and L. Nordström, *Physical review letters* **96**, 256601 (2006).
- [11] C.-T. Wu, O. T. Valls, and K. Halterman, *Phys. Rev. B* **86**, 184517 (2012).
- [12] J. Linder and J. W. A. Robinson, *Nat Phys* **11**, 307 (2015).
- [13] J. Kwo, M. Hong, and S. Nakahara, *Applied Physics Letters* **49**, 319 (1986).
- [14] W. Moffatt, G. E. C. Research, and D. C. T. M. Operation, *The Handbook of Binary Phase Diagrams*, The Handbook of Binary Phase Diagrams No. v. 4 (General Electric Company, Corporate Research and Development, Technology Marketing Operation, 1981).
- [15] M. Björck and G. Andersson, *Journal of Applied Crystallography* **40**, 1174 (2007).

- [16] P. Scherrer, Nachrichten von der Gesellschaft der Wissenschaften zu Göttingen, Mathematisch-Physikalische Klasse **1918**, 98 (1918).
- [17] J. Borchers, M. Salamon, R. Erwin, J. Rhyne, R. Du, and C. Flynn, Physical Review B **43**, 3123 (1991).
- [18] A. Di Bernardo, S. Diesch, Y. Gu, J. Linder, G. Divitini, C. Ducati, E. Scheer, M. G. Blamire, and J. W. A. Robinson, Nat Commun **6** (2015), 10.1038/ncomms9053.
- [19] V. Lauter-Pasyuk, H. J. Lauter, B. P. Toperverg, L. Romashev, and V. Ustinov, Phys. Rev. Lett. **89**, 167203 (2002).
- [20] J. D. S. Witt, T. P. A. Hase, R. Fan, C. J. Kinane, T. R. Charlton, S. Langridge, and M. G. Blamire, Journal of Physics: Condensed Matter **23**, 416006 (2011).
- [21] H. Zabel, Materials Today **9**, 42 (2006).
- [22] J. Lang, D. Lee, D. Haskel, and G. Srajer, Journal of applied physics **95**, 6537 (2004).
- [23] A. Paul, Scientific reports **6** (2016), 10.1038/srep19315.